Numerical Analysis of the Thermal Performance of Energy Diaphragm Walls

Rúben André Matos Sirgado

Instituto Superior Técnico
Lisboa, Portugal
ruben.sirgado@tecnico.ulisboa.pt

***Abstract*—The use of the energy stored inside the earth, know as low-enthalpy geothermal energy is increasing due to the global energy demand and need to decrease the consumption of fossil fuels. The exploitation of this renewable energy occurs with the help of ground source energy systems, within which underground structures such as, energy piles, tunnel linings or energy walls can be utilised. These geostructures are equipped with heat exchanger pipes with a circulating fluid that allows heat exchange with the ground. Studies relating to the use of energy walls are scarce due to their complexity and numerical demand. Using the finite element software FEFLOW, several three-dimensional thermal analyses were performed and compared to existing numerical and field studies to understand the software viability.**

Subsequently, a parametric study was performed to analyse the thermal impact of the mesh, heat exchanger layout, thermal conductivity of the soil, thermal conductivity of the wall and the geometry of the wall. The findings present that walls with greater exposure to the excavated space present greater heat transfer rate, followed by thermal conductivity of the soil and wall.

***Index Terms*—Energy walls, geothermal energy, renewable energy, finite element analysis, heat exchangers.**

I. Introduction

In recent decades we have seen an increase in global energy demand caused by the growth of the world's population and due to the pursuit of a better quality of life. To fulfill this demand, the consumption of fossil fuels increased significantly for the last decades [1], and since these fuels have a negative impact on the environment, there is the need to find a more environmentally sustainable source. As a result, to replace this energy the use of the heat stored in the ground most commonly known as geothermal energy, if adequately managed, can be a viable source to replace the non-ecological energies. To exploit this energy, ground source heat pump systems are used, this technology can either extract the energy directly from the groundwater (open-loop), or with heat exchanger pipes with a circulating fluid allows either extraction or heat injection (closed-loop). This study is focused around closed-loop systems incorporated in energy geostructures, these structures are commonly known as energy piles, tunnel linnings and energy walls. However, in recent years, interest in energy walls has seen a significant increase [1] in both numerical [2] [3] [4] [5] [6] [7] and [8] and field tests [9] and [10]. Consequently, this work aims to present different and complex finite element analysis with three-dimensional (3D) models to evaluate and gather numerical data. The main parameters studied are the different types of mesh, different heat exchanger layouts, the soil and wall thermal conductivity, and wall geometry.

II. Background

As mentioned before, energy walls are a recent form of energy foundation, that leads to a lack of long term data. Nevertheless, Brandl [10] states one particular case of a real life application of this technology since 2008 in Vienna, Austria, at the U2/2 metro line. This case presented a huge contribution with the insertion of approximately 103 km of heat exchanger pipes and an energy injection and extraction of approximately $175[MWh/year]$ and $437[MWh/year]$ respectively.

Xia [9], reports a field test performed in the Shanghai museum of natural history, located in China. The public building has a total of 452 W-shaped heat exchangers introduced in diaphragm walls with depths between 30 and 38 m. The author states that the increase of water velocity had a major impact on the heat exchanger rate and that W-shaped loops have a better performance than U-shaped loops. Several authors developed and validated numerical models with the data presented by Xia.

Di Donna [5] for example, performed a parametric study with the main objective of determining which design parameters are more effective in order to increase the energy performance of the energy wall, the author adopted the field values provided by Xia [9] and Sun [11]. The study concluded, in the short term pipe spacing proved to have a significant impact and in the long term, excess temperature which is the most impactfull parameter.

In contrast, in another numerical study, Markasis [2] presented a thermal behavior work regarding different pipe configurations, ground thermal properties and geometry of the wall and concluded that pipe spacing for deeper walls is

not that significant and it is independent of the soil thermal conductivity. This allows higher pipe spacing and less tubing, making energy walls a more economically viable structure.

III. Parametric Study

The numerical model adopted for this study is implemented with the finite element software FEFLOW, with 1D elements to recreate the heat exchanger pipes. A parametric study was performed where a set of parameters was studied: thermal impact of the mesh, heat exchanger layout, thermal conductivity of the soil, thermal conductivity of the wall and the geometry of the wall.

A. Model generation

In the first place, a finite-element mesh has to be generated to reproduce one viable model domain, therefore, a vertical cross-section needs to be defined first. In this phase, the user uses nodes and lines to define the dimensions and limits of the model. Every line needs to have a node at each end, and are used to establish a continuous alignment of mesh element edges that will be visible in the mesh after its generation. Afterward, the type of mesh needs to be defined by the user, and triangular elements were employed since the triangle has a better performance with complex geometries and the simulations run faster. In this phase, there is also the option of doing some mesh refinement. Following this process, the 2D model is converted into a 3D model, this process occurs with the insertion of a layered configuration. These layers can also be known as slices. The distance between slices can be changed by the user, the sum of these distances represents the model width. The 2D triangular elements are now prismatic six-noded 3D elements. After the 3D model is generated, the next step is always to define the problem class. In this phase, it's when the different settings of the project need to be provided in order to represent the 'reality'. Therefore, the flow was simulated with via standard groundwater-flow equation (saturated), and only transport of heat in a transient state was considered. When this is all set, the task of assigning model parameters occurs. Initial temperature, boundary conditions, material properties are assigned to the elements and element nodes. Finally, by selecting element edges it is possible to assign a special 1D special element named Discrete features, which represents a high-conductivity feature that can be used to represent tunnels, pipes, fractures and drains. These features are governed by three possible flow laws: Manning-Strickler, Hagen-Poiseuille, and Darcy. For this study the Hagen-Poiseuille law was considered since it refers to a flow of an incompressible and Newtonian fluid flowing through a cylindrical pipe of the constant cross-section. It is more suitable to represent the heat exchange pipes used in the energy diaphragm wall.

B. Model geometry and pipe configuration

The model geometry is proven to be one of the parameters with the biggest impact on the thermal performance of the wall, therefore, different geometries were defined with the different specifications presented in Table I. The geometries adopted considered different distances for values of excavation depth (D_e), depth of the wall (D_w), wall surface area (A), slab thickness (T_s) and wall thickness (T_w).

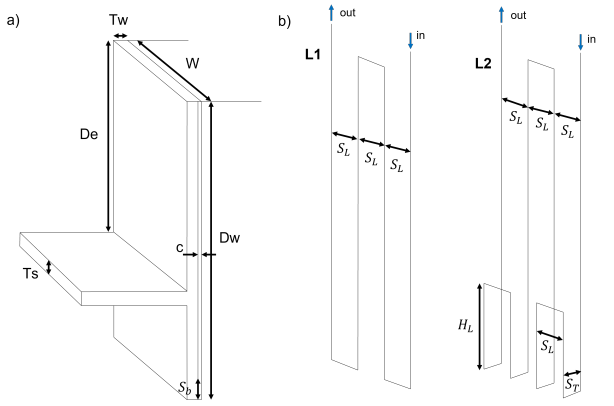

Fig. 1. Schematic representation: a) Diaphragm wall and slab and b) Pipe configuration L1 and L2

TABLE I
Geometric parameters of the wall for the parametric study

Geometry	D_e[m]	D_w[m]	T_w[m]	A[m^2]	T_s[m]
G10_5	10	15	0.6	24	0.6
G20_5	20	25	0.9	40	0.9
G30_5	30	35	1.2	56	1.2

Additionally, the diaphragm wall is incorporated with a slab to simulate real life scenarios such as underground parks and underground metro stations. Figure 1 presents a schematic representation of the energy wall.

According to Xia [9], W-shaped loops have a better performance than U-shaped loops, therefore W-shaped configurations were adopted for the following study however, one adopted extra tubing at the bottom, both layouts are presented in Figure 1. The parameters endorsed for the heat exchanger layouts were the spacing between vertical pipe, (S_p), a value of 0.4 m was adopted. The concrete cover to the pipes, (c), was set to be 0.1 m and a distance from the bottom slab face, (S_b), of 0.5 m. For the highest longitudinal pipe a distance of 1 m from the top boundary, (S_l) was adopted. For layout L2, the values adopted for the transverse spacing between vertical pipe branches (S_T) and the distance of the vertical loop on the embedded part of the wall (S_H), are defined depending on the geometry adopted. Therefore, the equations used to determine the values of these parameters are presented:

$$S_T = T_W - 2C \tag{1}$$

$$H_L = D_W - D_e - T_s - S_b \tag{2}$$

For the heat exchanger layout, the geometric parameters of cross sectional area (A) of 346.851mm^2, pipe outer diameter of 25 mm and pipe inner diameter of 20.4 m was considered.

C. Material Properties

The following study, the value of the thermal conductivity of the soil will assume values of 1.0 [W/m K], 2.0 [W/m K], and 3.0 [W/m K], the other material parameters are constant and the values assigned to the wall are the same for the slab. Table II lists the thermo-physical values of the materials.

D. Boundary conditions and initial thermal conditions

Firstly, for all the analyses, the same constant initial temperature of 17ºC is applied for the wall and soil. As for the boundary conditions, only the top part of the wall and the exposed part of the wall and slab were set with a temperature boundary condition, or the rest a no heat flux boundary was considered. For the latter, this means that at the nodes where this property is applied there is no heat loss or gain, which leads to a full isolation of the model. Since all simulations performed in the parametric study have a duration of 1095 days (3 years) a set of varying temperatures were considered for the temperature boundary conditions. To each, a sinusoidal equation was adopted, to represent the thermal behaviour of the energy wall for heating (winter) and cooling (summer) demand, which both depend on the external air temperature. Table III presents the assigned boundary, the temperature range for each boundary, and the sinusoidal equation considered, where d represents the time in days (between 0 and 365). Imposing a convective heat transfer through the wall, there is a the exchanged power, Q[W] and the heat transfer rate per square meter of wall, $q[W/m^2]$, these values can be calculated with the help of the following equations:

$$Q = mc_w(T_i - T_o) \tag{3}$$

$$q_L = \frac{Q}{L} \tag{4}$$

E. Meshing

The following study works with high temperature gradients close to the pipes, it is extremely important to secure a good refinement and considerable amount of elements since these are crucial parameters that can have a huge impact on the results. Therefore, a different set of meshes were reproduced to understand the behavior of the software. Table IV presents the different properties of each mesh reproduced. For the 3D configuration of the model, mesh type MI considered of 16 layers (17 slices) for a model width of 1.6 m was considered which leads to a distance of 0.1 m per layer, in contrast, mesh type MII considered a 24 layers (25 slices) for a model width of 1.6 m with distance between slices ranging from 0.01 m to 0.1 m. For mesh type MIII, due to computational requirements the results output was not possible to be obtained.

F. Runs performed

The parametric study will contain several simulations with the parameters presented in the previous sections. Table V summarises the different combinations that are adopted in this study, the geometry, mesh type, heat exchanger layout, soil thermal conductivity and the case name of the simulation are presented.

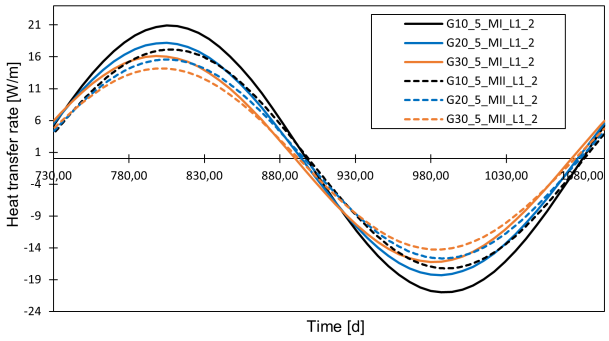

Fig. 2. Heat transfer rate evolution for the third year of simulation for mesh type MI and mesh type MII

IV. Results and Discussion

A. Influence of the mesh

Considering Table VI, the simulations used in this subsection to perform the mesh influence adopted the heat exchanger layout L1 and constant soil thermal conductivity of 2 $[W/mK]$. As expected, the values obtained for both meshes were different and with a considerable discrepancy. Figure 2 presents the results for the third year of simulation (from 730 days to 1095 days), in terms of heat transfer rate. Mesh type MII gave lower heat exchange values when compared to mesh type MI, in order to study these results the peak values for summer (cooling) and winter (heating) seasons were considered.

Considering the different meshes and geometries adopted the peak may vary with a range of 1 to 10 days. The peak values for heating and cooling are presented in Figure 3 for the three geometries in study. For cooling (summer) conditions a decrease of heat transfer rate is verified for each geometry, 21.9%, 16.7% and 14%, for heating (winter) properties the same behaviour was verified, 21.9%, 16.8% and 13.9% was verified to geometries G1, G2 and G3, respectively. The geometry with less excavation depth presented a bigger discrepancy of the values when compared to the others, a possibility for this outcome is that a greater excavation depth leads to a greater exposure to the exterior space boundary, which can lead to a stabilization of the values. The difference between cooling and heating is not significant, but considering the values obtained the following parameters studied the mesh type MII was adopted, in the subsequent analyses.

B. Influence of the heat exchanger layout

The next parameter to be discussed is the heat exchanger layout impact, both pipe configurations are presented in figure I. Both pipe configurations were adopted for each geometry with the same thermal conductivity of the soil, and therefore, it was possible to calculate the difference between results.

For the geometry G10_5, an increase of 4.2%, 6.3%, and 7.9% (heating and cooling) from pipe configuration L1 to L2

TABLE II
MATERIAL PROPERTIES OF THE WALL, SOIL AND HEAT CARRIER FLUID ADOPTED IN THE PARAMETRIC STUDY

	Geostructure	Soil	Heat Carrier Fluid
Porosity $n[-]$	0	0	-
Horizontal hydraulic conductivity, $k_x = k_z[m/s]$	0	0	-
Vertical hydraulic conductivity, $k_y[m/s]$	0	0	-
Bulk volumetric heat capacity, $c\rho[MJm^{-3}K]$	2.25	2.0	4.2
Bulk thermal conductivity, $\lambda[Wm^{-1}K^{-1}]$	2.0	1.0/2.0/3.0	0.6
Bulk density, $\rho[kgm^{-3}]$	2500	2000	1000
Longitudinal dispersivity, $\alpha_L[m]$	5	5	-
Transversal dispersivity, $\alpha_T[m]$	0.5	0.5	-

TABLE III
TEMPERATURE BOUNDARY CONDITIONS ADOPTED FOR THE PARAMETRIC STUDY

Location	Boundary	Temperature $[C]$	Equation
Exterior	Top boundary	17 ± 6	$T_{ext}(d) = 17 + 6sin(2\pi d/365)$
Interior	Slab and wall surface	17 ± 3	$T_{int}(d) = 17 + 3sin(2\pi d/365)$
Inlet	Inlet node	17 ± 10	$T_{inlet}(d) = 17 + 10sin(2\pi d/365)$

TABLE IV
PROPERTIES OF THE MESHES USED IN THE PARAMETRIC STUDY.

Mesh	#Elements	#Nodes	#Layers	#Nodes per slice	#Slices
G10_5-MI	86768	48178	16	2834	17
G20_5-MI	106672	59364	16	3492	17
G30_5-MI	139552	76959	16	4527	17
G10_5-MII	220714	116262	26	4306	27
G20_5-MII	347464	182142	26	6746	27
G30_5-MII	549952	289872	26	10736	27
G20_5-MIII	758320	395158	40	9638	41

was verified for a soil thermal conductivity of 1.0, 2.0 and 3.0$[W/mK]$, respectively. For geometry G20_5 an increase of 3%, 4.6%, and 5.8% (heating and cooling) was observed for the same thermal conductivities 1.0, 2.0 and 3.0$[W/mK]$. In general, the values for heat transfer rate for heat exchanger layout L2, presented higher values when compared to L1, also, when geometry G20_5 was performed the increase was slightly lower when compared to geometry G10_5. In addition, as expected the values obtained for higher soil thermal conductivity presented a higher increase since the fluid spends more time inside the tubes.

C. Influence of the thermal conductivity of the soil

Regarding the thermal conductivity of the soil, as expected the values for higher thermal conductivity lead to the highest values for heat transfer rate. Additionally, these simulations were performed for heat exchanger layout L1 and L2. As for configuration L1, it was possible to obtain figure 5, which translates the values obtained for heat transfer rate for the peak values, with the varying soil thermal conductivity of 1.0 [W/mK], 2.0 [W/mK] and 3.0 [W/mK] and wall geometries G10_5, G20_5 and G30_5.

Taking the simulations with soil thermal conductivity equal to 1.0 [W/mK], when this value is increased to 2.0 [W/mK], for cooling (summer) geometries G10_5, G20_5, and G30_5 presented an increase of 8.7%, 8.9%, and 9.8% respectively and for heating (winter), the same geometries present a similar

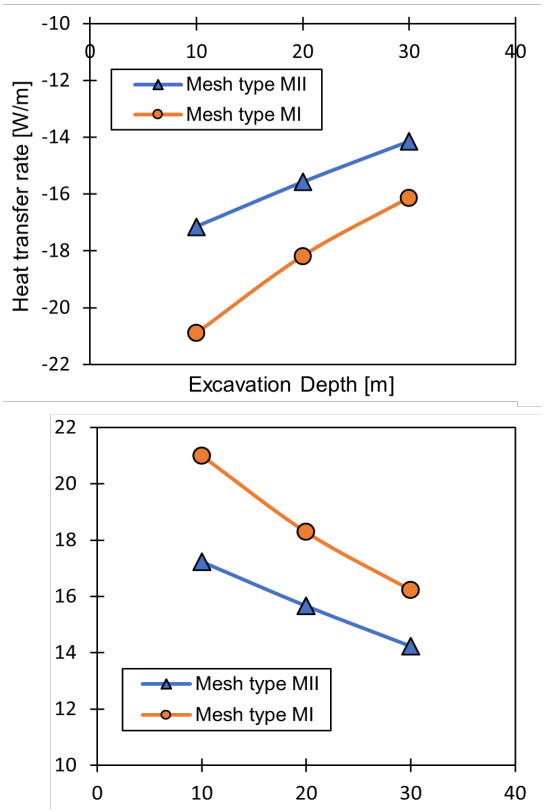

Fig. 3. Heat transfer rate evolution for the peak values of heating (left) and cooling (right) for third year of simulation for mesh type MI and mesh type MII

increase, 8.8%, 9%, and 9.9%, respectively. For the increase of 50% of the soil thermal conductivity, 2.0 [W/mK] to 3.0 [W/mK], an increase in heat transfer rate of 5.9%, 6.1%, and 7% (cooling) and 5.9%, 6.1%, and 6.9% (heating) is verified for G10_5, G20_5 and G30_5 respectively. However, as mentioned before for pipe configuration L2 due to computational requirements, simulations with wall geometry G30_5 were not performed. Therefore, Figure 6 only presents values for G10_5

TABLE V
CASES PERFORMED IN THE PARAMETRIC STUDY

Geometry	Mesh Type	Heat Exchanger Layout	Thermal Conductivity of the soil, $\lambda[W/m/K]$	Case Name
G1	MI	L1	1.0	G1_MI_L1_1.0
			2.0	G1_MI_L1_2.0
			3.0	G1_MI_L1_3.0
		L2	1.0	G1_MI_L2_1.0
			2.0	G1_MI_L2_2.0
			3.0	G1_MI_L2_3.0
	MII	L1	1.0	G1_MII_L1_1.0
			2.0	G1_MII_L1_2.0
			3.0	G1_MII_L1_3.0
		L2	1.0	G1_MII_L2_1.0
			2.0	G1_MII_L2_2.0
			3.0	G1_MII_L2_3.0
G2	MI	L1	1.0	G2_MI_L1_1.0
			2.0	G2_MI_L1_2.0
			3.0	G2_MI_L1_3.0
		L2	1.0	G2_MI_L2_1.0
			2.0	G2_MI_L2_2.0
			3.0	G2_MI_L2_3.0
	MII	L1	1.0	G2_MII_L1_1.0
			2.0	G2_MII_L1_2.0
			3.0	G2_MII_L1_3.0
		L2	1.0	G2_MII_L2_1.0
			2.0	G2_MII_L2_2.0
			3.0	G2_MII_L2_3.0
G3	MI	L1	1.0	G3_MI_L1_1.0
			2.0	G3_MI_L1_2.0
			3.0	G3_MI_L1_3.0
		L2	1.0	G3_MI_L2_1.0
			2.0	G3_MI_L2_2.0
			3.0	G3_MI_L2_3.0
	MII	L1	1.0	G3_MII_L1_1.0
			2.0	G3_MII_L1_2.0
			3.0	G3_MII_L1_3.0
		L2	1.0	G3_MII_L2_1.0
			2.0	G3_MII_L2_2.0
			3.0	G3_MII_L2_3.0

and G20_5. The values for thermal conductivity increase from 1.0 [W/mK] to 2.0 [W/mK] presented an increase of 10.7% and 10.4% (cooling), and of 10.8% and 10.5% (heating) for geometries G10_5 and G20_5 respectively. For 2.0 [W/mK] to 3.0 [W/mK], this increase translate into 7.5% and 7.3% (heating and cooling) for G10_5 and G20_5. It can be recognized that the variation of the peak values obtained with the pipe configuration L2 was slightly higher, which can conclude that if the water spends more time in the tubes, the thermal conductivity of the soil has a bigger impact.

D. Influence of the thermal conductivity of the wall and soil together

Several authors present studies where the conductivity of the concrete is one of the most important parameters regarding energy walls (Di Donna, 2017; Di Donna, 2021). A baseline value of concrete thermal conductivity of 2.0 $[W/mK]$ has been used previously and here values of 1.0, 2.0, and 3.0$[W/mK]$ were utilised. In Figure 7, the results (coloured lines) are compared to the analyses where only the soil thermal conductivity was varied (black lines), and as the cooling values presented no significant differences when compared to the heating, the same conclusions can be made. Upon analyzing the chart, it can be observed a huge impact for the decrease of thermal conductivity of the wall from 2.0 $[W/mK]$ to 1.0 $[W/mK]$ and heat exchanger layout L1, a decrease of 59%, 54% and 46% was observed for geometries G10_5, G20_5, and G30_5 respectively.

As for, the increase of the thermal conductivity of the wall from 2 $[W/mK]$ to 3 $[W/mK]$ an increase of 24%, 22%, and 20% for geometries G10_5, G20_5, and G30_5, respectively, for heat exchanger layout L2, the variation presented approximately the same range.

The variation of the values obtained for thermal conductivity of 1.0[W/mK] presented to be extremely impactful and for thermal conductivity of 3.0[W/mK] the values presented to be significant as well. One important relation was found, less excavation depth leads to a higher influence on the results, which means less wall length and less time that fluid spends inside the heat exchanger pipes.

E. Influence of the wall geometry

To assess the impact of the geometry in the thermal performance of the diaphragm wall, a new set of simulations was performed. For each of them, mesh type MII is used as well as the heat exchanger layout L1, for soil and wall thermal

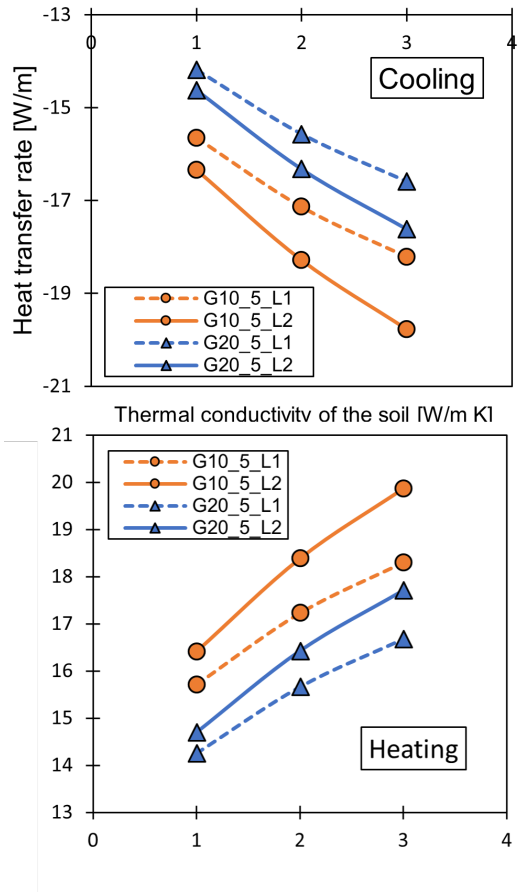

Fig. 4. Heat transfer rate for the peak values of the third year of the simulation for heat exchanger layout L1 and L2

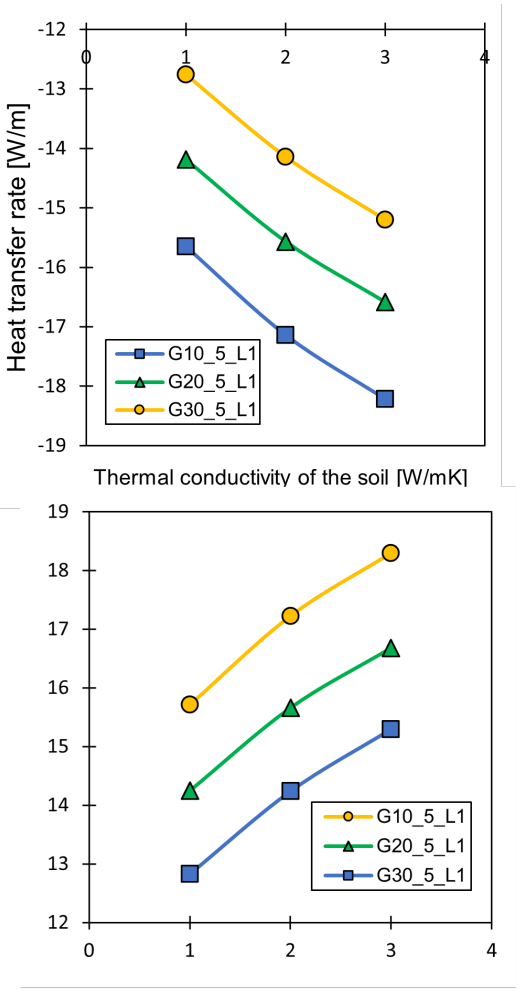

Fig. 5. Heat transfer rate for the peak values of the third year of the simulation for the different thermal conductivities and heat exchanger layout 1

conductivity a constant value of 2 $[W/m/K]$ is established. The aim was to reproduce different model configurations in order to understand the impact of each parameter, wall thickness T_w, and ratio between excavation depth and buried depth (De/Db) are studied. Therefore, values for T_w of 0.6$[m]$, 0.9$[m]$ and 1.2$[m]$ were used, and for De/Db values of 0, 1, 2, 4, 6 and infinite were considered. Table VI presents the new geometries and their specifications for excavation depth (D_e), buried depth (D_b), ratio between excavation depth and buried depth studied (De/Db), wall surface area (A_w) and wall thickness (T_w).

The results are presented in Figure 8, to which trend lines for each value of T_w were inserted for each thickness, to represent the results obtained for De/Db=infinity the value of 10 was adopted. As expected, the values for wall thickness of 1.2$[m]$, lead to a greater distance between the heat exchange pipes and the interior boundary condition, therefore, less variation and lower values for heat exchanger rate when compared to thicknesses of 0.6$[m]$ and 0.9$[m]$ are verified. For T_w=1.2m the difference between De/Db=1 to De/Db=Infinite presented a value of only 1.3%. For geometries with higher De/Db ratio, a higher heat exchanger rate was verified, since greater ratios led to a higher exposure of the wall to the interior space boundary. Regarding the T_w=0.9$[m]$, a smaller wall thickness led to higher heat exchanger rate values, the same relations mentioned above were verified. However, a larger increase was verified when comparing lower De/Db ratio with higher values, the difference between De/Db=1 to De/Db=Infinite was 8.1% . For the smallest wall thickness, the dissimilarity between heat exchange values as a function of De/Db was further accentuated, values with less exposure to the interior space (De/Db) presented lower heat transfer rate, nevertheless, for the other De/Db relations, the amount of heat transferred is higher when compared to the other thicknesses.

Figure 9 represents screen shots of heat flow field for Case G10_0 (a) and G20_0 (b). For this plots, the coloured marks represent the heal flow (W) at each node which depends on the adjacent elements size. The interior boundary the marks are in the green-light blue range for G10_0, and represent lower heat flow values than case G20_0 (light blue and dark blue), Figure 9. The arrows added to the figure illustrate the direction of the heat flow at the boundaries, i.e. into the soil from the top surface and from the wall to the interior space.

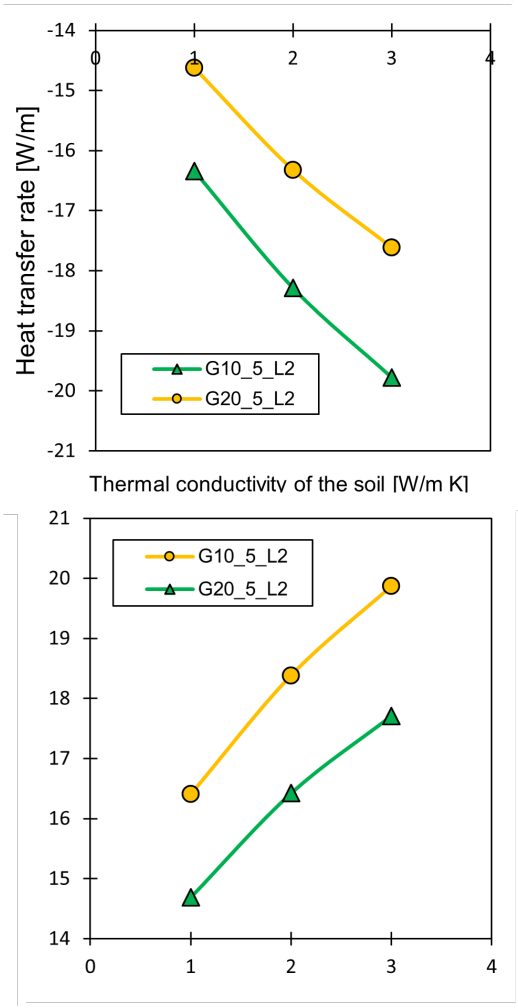

Fig. 6. Heat transfer rate for the peak values of the third year of the simulation for the different thermal conductivities and heat exchanger layout 2

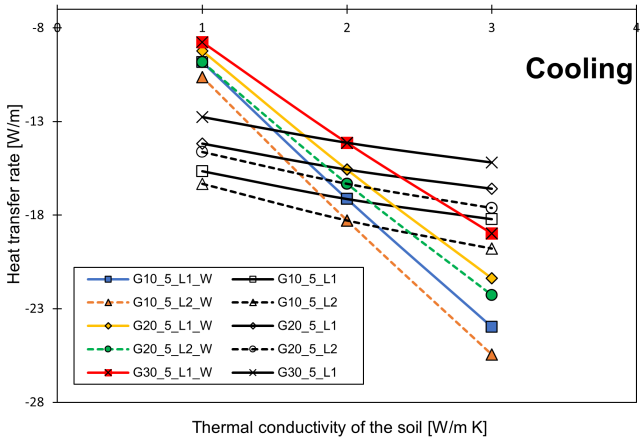

Fig. 7. Heat transfer rate for the peak values of the third year of the simulation for the different thermal conductivities of the wall

TABLE VI
PROPERTIES OF THE GEOMETRIES ADOPTED IN THE PARAMETRIC STUDY

-	$D_e[m]$	$D_b[m]$	D_e/D_b	$A_w[m^2]$	$T_w[m]$
G10_0_0.6	10	0	INF	16	0.6
G0_10_0.6	0	10	0	16	0.6
G10_5_0.6	10	5	2	24	0.6
G10_10_0.6	10	10	1	32	0.6
G16_4_0.6	16	4	4	32	0.6
G20_0_0.6	20	0	INF	32	0.6
G0_25_0.6	0	25	0	40	0.6
G20_10_0.6	20	10	2	48	0.6
G20_0_0.9	20	0	0	32	0.9
G16_4_0.9	16	4	4	32	0.9
G20_5_0.9	20	5	4	40	0.9
G20_10_0.9	20	10	2	48	0.9
G10_10_0.9	10	10	1	32	0.9
G30_5_1.2	30	5	6	56	1.2
G28_7_1.2	28	7	4	56	1.2
G20_0_1.2	20	0	INF	32	1.2
G0_25_1.2	0	25	0	40	1.2

This is consistent with the temperature fields shown in Figure 10 (a) and (b). Comparing the temperature fields for the two cases, it appears that the ground is warmer, further from the pipes to the soil and thus, would help explain the reduced heat exchanged. It is not entirely clear why the heat exchange to the interior is reduced but it may be due to a general warming of the wall section as well as the soil, and reduced thermal gradients in this direction as well.

V. CONCLUSIONS

Considering the analyses discussed above the following conclusions can be made:

- The meshes with more nodes, elements and symmetrical characteristics presented way more precision on the results output, a difference of only 1.4% was verified for the finner and more complex meshes.
- The soil thermal conductivity presented to be a significant parameter regarding energy diaphragm walls, an average increase of 10.6% between $1.0[W/mK]$ and $2.0[W/mK]$ and 7.4% between $2.0[W/mK]$ and $3.0[W/mK]$;
- Changing the concrete thermal conductivity affects the heat transfer rate in a considerable way, where an average increase of 54% between $1.0[W/mK]$ and $2.0[W/mK]$ and 22% between $2.0[W/mK]$ and $3.0[W/mK]$;
- The wall geometry, presented that the energy walls with higher ratio between excavated distance and buried distance provide an increase of heat transfer rate. This parameter presented a relation with the thickness of the wall, for higher thicknesses the ratio of excavated distance and buried distance was less predominant when compared to thinner walls. For geometries adopting total exposure to the interior space, the deepest walls presented higher values of heat exchanger rate since there is a higher wall area. The difference between relation of excavated distance and buried distance for total exposure and total embeddement of the wall for higher thicknesses was near 1%, however, for smallest thickness presented in this study an increase of 34% was verified.

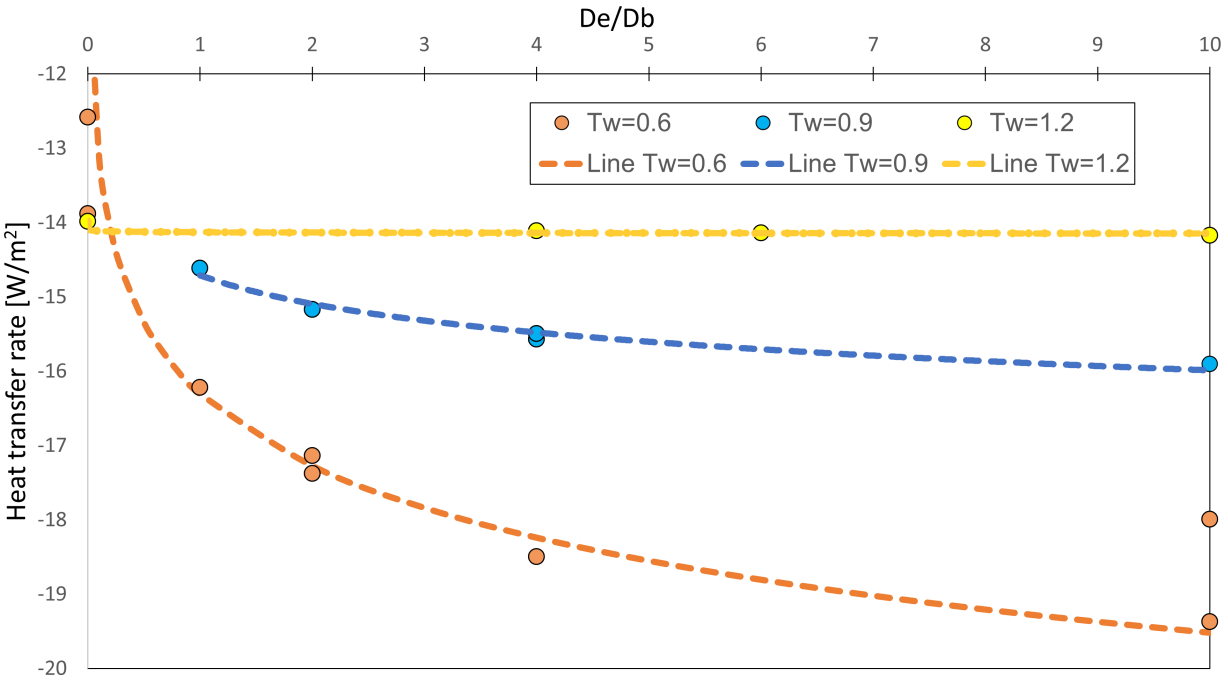

Fig. 8. Effect of the different wall geometries in the heat exchanger rate.

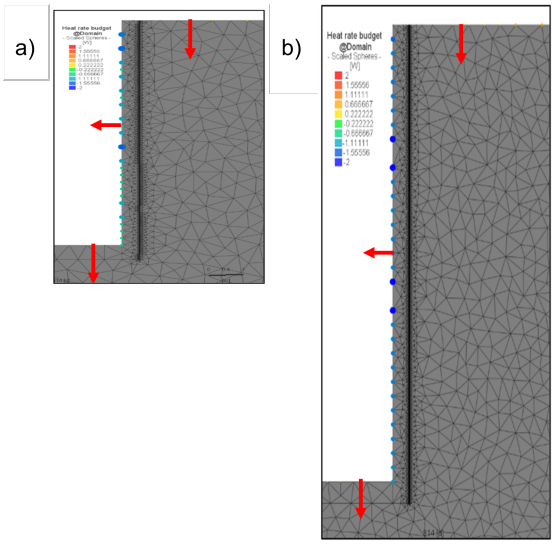

Fig. 9. Heat transfer rate for geometry: G10_0 (a) and G20_0 (b)

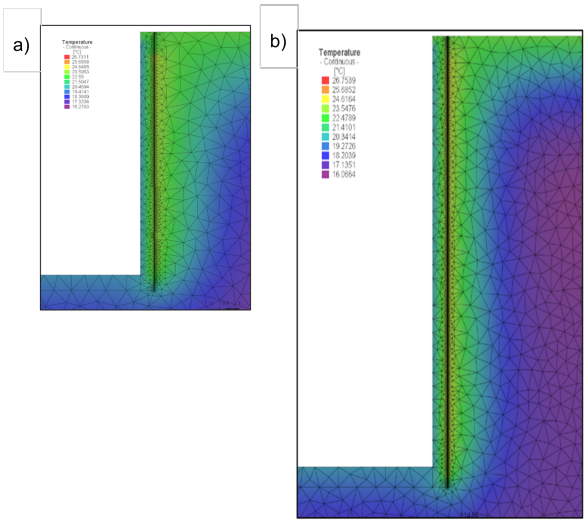

Fig. 10. Temperature gradient for geometry: G10_0 (a) and G20_0 (b)

VI. Acknowledgements

This work was carried out in Instituto Superior Técnico with an educational license for the MIKE Powered by DHI Software FEFLOW that allowed to perform the numerical analysis presented.

References

[1] Laloui, L., & Rotta Loria, A. F. (2020). Energy geostructures. In Analysis and Design of Energy Geostructures (pp. 25–65). Elsevier. https://doi.org/10.1016/B978-0-12-816223-1.00002-3

[2] N. Makasis, G. A. Narsilio, A. Bidarmaghz, I. W. Johnston, and Y. Zhong, "The importance of boundary conditions on the modelling of energy retaining walls," Computers and Geotechnics, vol. 120, p. 103399, 2020.

[3] M. Sun, C. Xia, and G. Zhang, "Heat transfer model and design method for geothermal heat exchange tubes in diaphragm walls," Energy and buildings, vol. 61, pp. 250–259, 2013.

[4] A. Di Donna, F. Loveridge, M. Piemontese, and M. Barla, "The role of ground conditions on the heat exchange potential of energy walls," Geomechanics for Energy and the Environment, vol. 25, p. 100199, 2021

[5] A. Di Donna, F. Cecinato, F. Loveridge, and M. Barla, "Energy perfor-

mance of diaphragm walls used as heat exchangers," Proceedings of the Institution of Civil Engineers-Geotechnical Engineering, vol. 170, no. 3, pp. 232–245, 2017

[6] M. Barla, A. Di Donna, and A. Santi, "Energy and mechanical aspects on the thermal activation of diaphragm walls for heating and cooling," Renewable Energy, vol. 147, pp. 2654–2663, 2020.

[7] N. Makasis and G. A. Narsilio, "Energy diaphragm wall thermal design: The effects of pipe configuration and spacing," Renewable Energy, vol. 154, pp. 476–487, 2020.

[8] E. Sailer, "Numerical modelling of thermo-active retaining walls," Ph.D. dissertation, PhD thesis. Imperial College London, 2020.

[9] C. Xia, M. Sun, G. Zhang, S. Xiao, and Y. Zou, "Experimental study on geothermal heat exchangers buried in diaphragm walls," Energy and Buildings, vol. 52, pp. 50–55, 2012.

[10] H. Brandl, "Energy foundations and other thermo-active ground structures," Geotechnique ´ , vol. 56, no. 2, pp. 81–122, 2006.

[11] Sun, M., Xia, C., & Zhang, G. (2013). Heat transfer model and design method for geothermal heat exchange tubes in diaphragm walls. Energy and Buildings, 61, 250–259. https://doi.org/10.1016/j.enbuild.2013.02.017